Oxidation of Metals, Vol. 64, Nos. 1/2, August 2005 (© 2005)
DOI: 10.1007/s11085-005-5705-2

High-Temperature Oxidation of an Aluminized NiCr Alloy formed by a Magnetron-Sputtered Al Diffusion Coating

J.-M. Brossard,* J. Balmain,*‡ F. Sanchette,† and G. Bonnet*

Received June 16, 2004; revised March 2, 2005

Aluminium diffusion coatings were obtained on Ni–20Cr substrate by sputtering an aluminium film, followed by a two stage diffusion treatment in an argon inert gas atmosphere (first stage at 600°C, second at 900 or 1100°C). Aluminides obtained at 900°C and 1100°C are close to those obtained by pack cementation process with high aluminium activity. These diffusion coatings are able to develop alumina scales during isothermal oxidation at high temperatures, whereas the untreated substrate had a chromia-forming behaviour. The weight gain recorded at 1100°C on coated sample is then smaller than the one of uncoated NiCr at 950°C. Presence of chromium was detected in the diffusion coating and Cr-rich precipitates were observed at the diffusion coating/substrate interface. After oxidation at 900°C and 1100°C, only α-Al_2O_3 was revealed by XRD. An intermediate scale with a "whiskered" morphology could however be observed after 48 hr oxidation at 900°C. After 100 hr of oxidation at 1100°C, the Ni_xAl_y diffusion phases were no longer detectable and the upper part of the oxide scale spalled away during cooling. Large cavities appeared at the initial location of the diffusion coating/substrate interface.

KEY WORDS: high-temperature oxidation; PVD; diffusion coating; NiCr alloy; aluminide.

*Laboratoire d'Etude des Matériaux en Milieux Agressifs, Pôle Sciences et Technologie, Bâtiment Marie Curie, 25 rue Enrico Fermi, 17000 La Rochelle, France
†Laboratoire des Procédés de Traitement de Surface, CEA DTEN/SMP, F38054 Grenoble cedex 9, France
‡To whom correspondence should be sent. e-mail: josseline.balmain@univ-lr.fr

INTRODUCTION

The high temperature oxidation behaviour of NiCr alloys has been extensively studied[1–4] and they are used for many industrial applications because of their high oxidation resistance and good mechanical properties at temperatures below 950°C. Above this temperature, the reaction between the external chromia scale and oxygen can form gaseous chromium oxides (CrO_3, ...) that points out the insufficient oxidation resistance of chromia-forming alloys at such temperatures. Various studies have been carried out on the effect of the addition of aluminium to M-Cr (M = Fe, Ni, Co) alloys as a third element to promote formation of protective Al_2O_3 scales thus improving the high temperature oxidation resistance.[4–8] The pursuit in increasing the operating temperature (>1000°C), especially for aero-engines, led to the development of MCrAlY superalloys (with M = Fe, Ni, Co),[8,9] which present high strength resistance. The amount of Al has to be sufficient to form and maintain an alumina protective scale during oxidation (%Al > 8–10 wt.% for M-Al and %Al >3–4 wt.% for M–20%Cr). In order to insure sufficient Al contents, protection of alloys is usually reinforced by nickel aluminide diffusion coatings.[9–12] These coatings are an effective way to increase the oxidation resistance by formation of a protective slow-growing alumina scale.[13–16] Aluminide diffusion coatings are widely obtained by pack cementation or by CVD and the mechanisms of coating formation, depending on parameters such as Al activity, temperature or time, are well documented.[17–22] Some works have demonstrated that physical vapour deposition (PVD) techniques can also be used to obtain aluminide coatings.[23–25] Recently, He *et al.*[25]directly applied Ni-Al coatings of determined composition by different PVD techniques, while Chu *et al.*[26] increased Al contents at the outer surface of TiAl alloys by depositing an Al film by sputtering, followed by a heat treatment. Various mechanisms of diffusion of the different elements from coating and substrate have been proven to govern the aluminide phase growth and coating microstructure.[27–28]

In this study, thin aluminium films were first deposited on Ni-20Cr alloy by magnetron sputtering and this deposited aluminium was then incorporated into the substrate by an appropriate heat treatment. Interdiffusion phenomena, taking place during the heat treatment step and leading to the formation of aluminide coatings, were investigated. Coated and uncoated specimens were finally subjected to isothermal oxidation at 900°C, 950°C or 1100°C, in synthetic air at the atmospheric pressure, and their oxidation behaviours were compared.

EXPERIMENTAL PROCEDURES

Material

Specimens were cut from a NiCr alloy rod (Ni–20Cr–1.5Si (wt.%)) with approximately 12 mm in diameter and 1.5 mm in thickness. Samples were abraded from 600 grit SiC to 1 μm diamond paste and then ultrasonically cleaned in ethanol before further use.

Deposition Conditions

Aluminium was deposited as thin films on all the surfaces of the NiCr substrates by DC cathodic magnetron sputtering technique. The employed sputtering conditions are summarised in Table I.

Thermal Treatment

After aluminium deposition, an interdiffusion thermal treatment was performed in a microbalance (SETARAM TGA92) under an Ar inert gas atmosphere. The chosen treatment consisted in a progressive heating up to 600°C, at 10°C/min, for a dwelling time of 1 hr, followed by a similar ramp to oxidation test temperature, where it was maintained for 15 min. Some specimens were cooled down to room temperature (10°C/min) after each stage in order to determine phase evolution.

High Temperature Oxidation Conditions

For coated samples, isothermal oxidation tests were performed under synthetic air atmosphere (80 vol.%N_2–20 vol.%O_2), after a complete

Table I. Main Sputtering Deposition Conditions

Substrate	Ni-20Cr–1.5Si (wt.%) Ni-22Cr–3Si (at.%)
Target	Al (99.9%)
Distance between target and substrate	70 mm
Pre-sputtering time	15 min
Working pressure	0.5 Pa
DC power	2.5 kW
Ar flow rate	80 sccm
Deposition rate	20 μm/hr
Bias	−50 V
Deposition time	8 – 10 min
Coating thickness	around 3 μm

diffusion heat treatment, as previously described (but without a cooling step), during 48 hr and 90 hr at 900°C or 1100°C. The raw substrates were heated at 10°C/min to the oxidation temperature under an Ar inert gas atmosphere, then oxidised under reconstituted air at 900°C or 950°C, temperatures low enough to avoid the volatilisation of Cr_2O_3 which can occur above the latter temperature. Weight changes due to oxidation were recorded by thermogravimetry.

Analytical Characterisation

A Brüker AXS X-Ray diffractometer, using Cu K_α radiation ($\lambda = 0.15406$ nm), was used (at 5° fixed angle) to identify the phases formed by the interdiffusion treatment and after oxidation at 900°C. An Inel G300 X-Ray diffractometer, equipped with a curved detector, was used at a grazing angle of 5° to characterise both the as-deposited Al film and the phases formed after oxidation at 1100°C, using Co K_α radiation ($\lambda = 0.1789$ nm). The as-deposited film morphology was characterised by atomic force microscopy (AFM CP-R Scanning probe microscope from Veeco Instruments) in contact mode. The surface morphologies and cross sectional microstructures of samples were observed by scanning electron microscopy (SEM - Jeol JSM 541 LV). The samples observed in cross-section were previously coated by electro-deposited nickel to protect the external surface during metallographic preparation. Energy dispersive X-ray spectrometry (EDS) was employed to determine the semi-quantitative compositional profiles (corrected by a Jeol ZAF program) across the coating. The lines of analysis were carried out diagonally across the coating and the oxide products and were further projected on one axis perpendicular to the surface.

RESULTS

As Deposited Aluminium Coating

The thickness of deposited aluminium films is around 3 μm. The films are found to be well crystallised, with a face centred cubic structure (JCPDS 89-2837, a = 0.4059 nm) according to XRD. Figure 1 consists of an AFM image showing the morphology of the as sputtered Al film. Deposit is constituted of nanosized nodules with small superficial cavities.

Diffusion Treatment

According to the aluminium-nickel phase diagram (Fig. 2), several intermetallic phases can be formed from an Al–Ni diffusion couple.

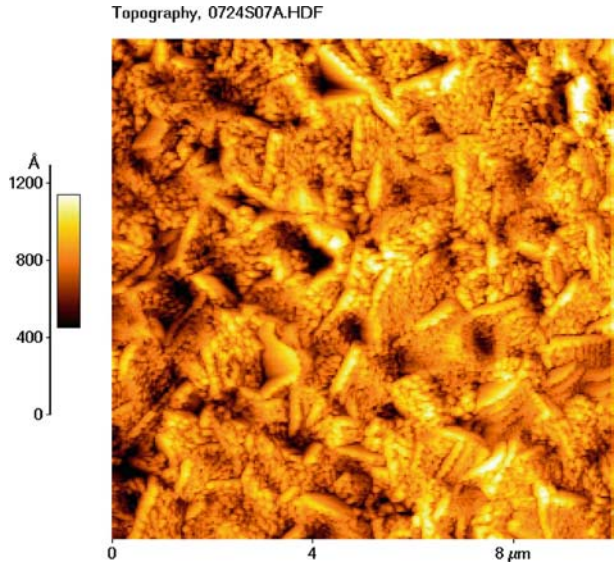

Fig. 1. AFM image of as sputtered Al film on Ni-20Cr–1.5Si (wt.%).

Among these, three present extended composition ranges (δ-Ni_2Al_3, β-NiAl and γ'-Ni_3Al) and one has a very narrow composition range ($NiAl_3$). In order to promote intermetallic phase formation on Ni–20Cr substrate, a thermal treatment was conducted on deposited samples. The first stage was carried out at 600°C to promote Al diffusion into substrate, thus avoiding melting of the pure Al-deposited layers that occurs at approximately 660°C.[29]

XRD analysis of coated sample treated 1 hr at 600°C under an inert Ar gas atmosphere (Fig. 3a) indicates that hexagonal δ-Ni_2Al_3 (JCPDS 65-3454) is the predominant phase although the substrate contribution is still detected. The corresponding SEM back-scattered electron image (BEI) of the polished section is presented on Fig. 4a. The diffusion zone has a uniform thickness (5 μm) without cracks or voids. The EDS composition profile (Fig. 4b) points out the presence of oxygen at the external interface. Oxide scale (0.5 μm) formation probably occurred at the gas/sample interface during heat treatment, in agreement with the corresponding recorded mass gain. The concentration profile shows that the Al content is comprised between 55 and 70 at.%, which is consistent with phase diagram presented in Fig. 2 ($NiAl_3 + Ni_2Al_3$, Ni_2Al_3 and $Ni_2Al_3 + NiAl$ (Al rich)). Moreover, chromium is always detected in the diffusion zone. The atomic

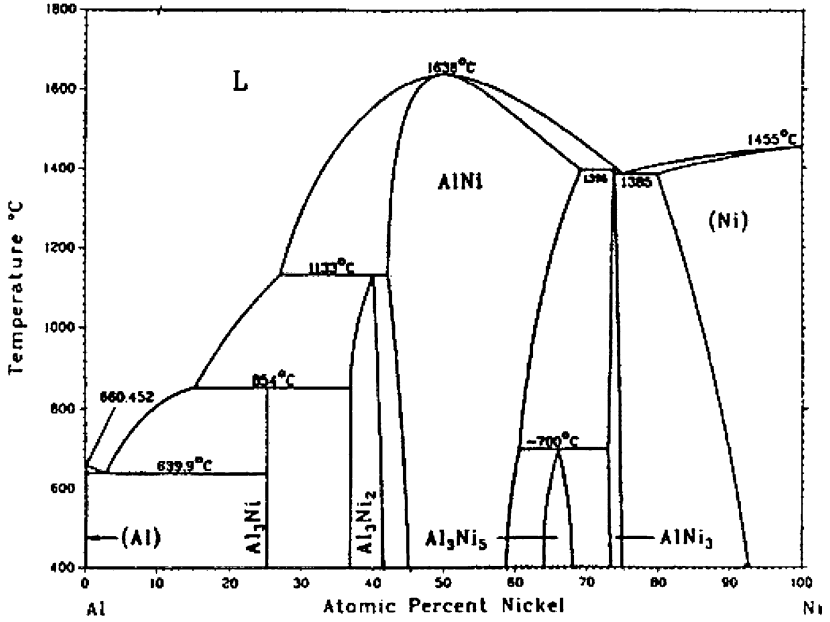

Fig. 2. Aluminium–nickel phase diagram [29].

ratio Cr/(Ni + Al) is around 0.1, which indicates that the Cr content is greater in the substrate (around 0.3) than in the diffusion coating.

X-Ray Diffraction patterns for samples after the second heat treatment stage, at 900°C and 1100°C, are presented on Figs. 3b and 3c, respectively. For samples treated at 900°C, the diffusion zone is principally constituted of β-NiAl with traces of δ-Ni_2Al_3 and $\gamma'Ni_3Al$ whereas, in the case of samples treated at 1100°C, it is mainly composed of β-NiAl and γ'-Ni_3Al and δ-Ni_2Al_3 is no more detected. The Ni20Cr substrate is still observed after treatment at 900°C but not after the treatment at 1100°C. Some small peaks can also be attributed to Al_2O_3 traces. An external oxide scale, partially detached from the surface, is observed on both samples treated at 900°C and 1100°C (Figs. 5a and 6a). For the sample treated at 900°C, the diffusion zone under the oxide is constituted of an uniform (5 μm) layer of Ni–Al. The Al concentration in this layer is around 43 at.% and slightly decreases between 5 and 7 μm from the surface. The atomic ratio Cr/(Ni + Al) is comparable with the one calculated after the first stage of the heat treatment. An elongated precipitate zone rich in Cr (3μm) can also be observed under the outer zone. The Al concentration drastically decreases in this latter region and the

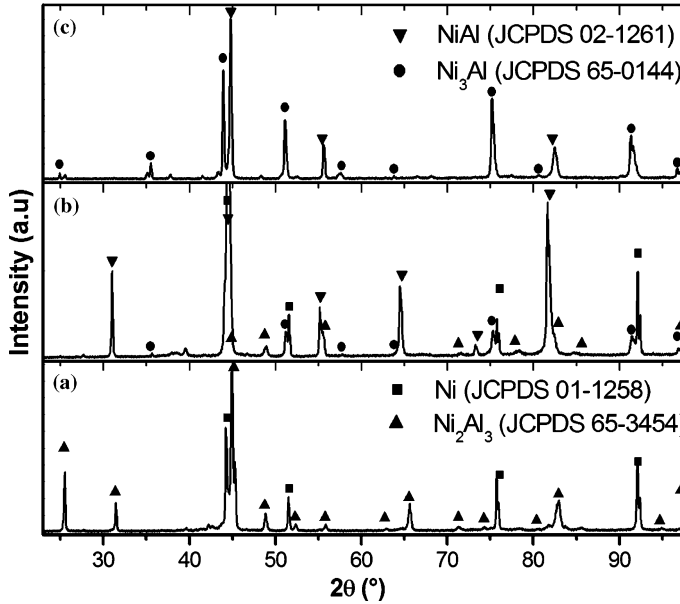

Fig. 3. XRD diffraction ($K\alpha_{(Cu)}$, $\theta = 5°$) patterns of Ni-20Cr–1.5Si (wt.%) with sputtered Al film (3 μm) after first step at 600°C (a), after second step at 900°C (b), after second step at 1100°C (c).

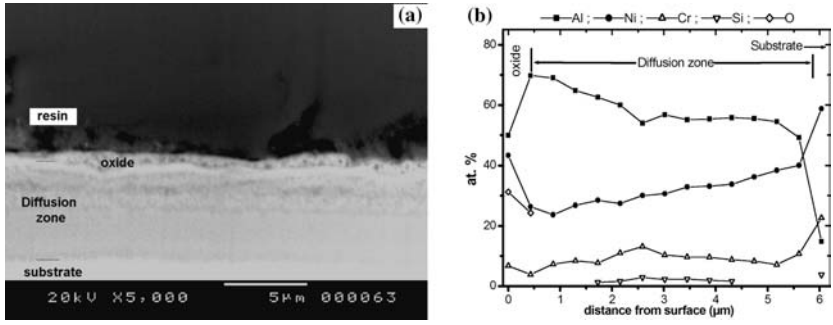

Fig. 4. Cross-section BSE image (a) of Ni-20Cr–1.5Si (wt.%) with 3 μm Al deposit after first step of heat treatment at 600°C, (b) corresponding EDS concentration profile.

composition of the substrate is found beyond it. The diffusion zone of sample treated at 1100°C is wider than the one on the sample treated at 900°C (7 μm instead of 5 μm). Two zones with different intensity contrasts are observed. EDS analysis (Fig. 6b) indicates that the Al content in the darkest zone is about 35 at.% and decreases to 20 at.% in the brighter

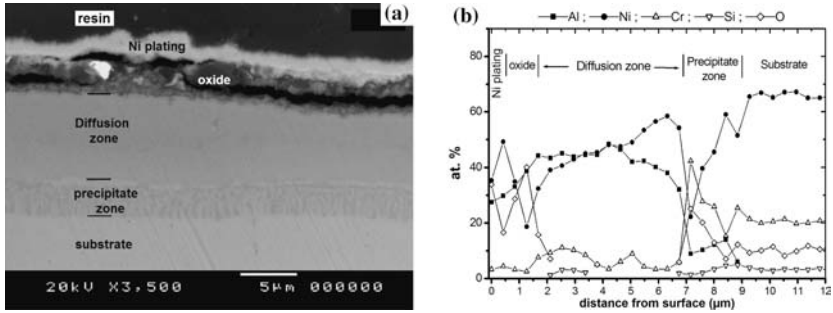

Fig. 5. Cross-section BSE image (a) of Ni-20Cr–1.5Si (wt.%) with 3 μm Al deposit after second step of heat treatment at 900°C, (b) corresponding EDS concentration profile.

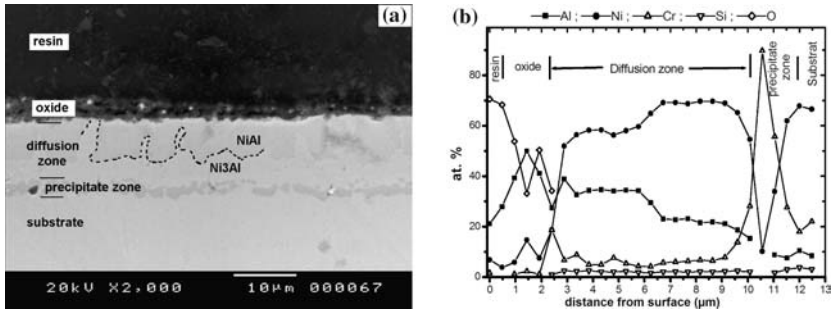

Fig. 6. Cross-section BSE image (a) of Ni-20Cr–1.5Si (wt.%) with 3 μm Al deposit after second step of heat treatment at 1100°C, (b) corresponding EDS concentration profile.

zone. A Cr-rich precipitate zone with a few small cavities can also be observed under the diffusion zone and the concentration ratio indicates that Cr content is around 7 at.%.

Oxidation

The isothermal oxidation kinetic curves for uncoated samples, oxidised at 900°C and 950°C, and coated samples, oxidised at 900°C and 1100°C, are presented in Fig. 7. At 900°C, the mass gains for coated and uncoated samples are comparable after 90 hr of oxidation. The oxidation kinetic curves of raw substrate and coated sample oxidised at 900°C are well fitted by a complete law including a linear term and a parabolic one:

$$t = cnst + \frac{1}{k_l}\left[\frac{\Delta M}{S}\right] + \frac{1}{k_p}\left[\frac{\Delta M}{S}\right]^2$$

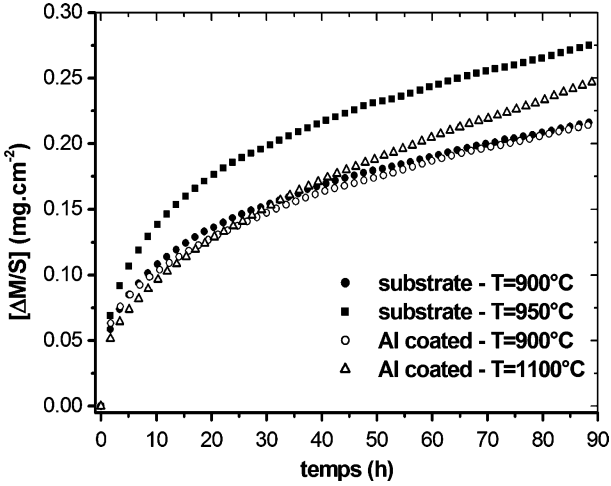

Fig. 7. Weight gain curves of Ni-20Cr–1.5Si (wt.%) oxidised at 900 and 950°C and of coated sample oxidised at 900 and 1100°C.

with t corresponding to the oxidation time, ΔM to the weight gain due to the oxidation, S to the sample surface area, and k_l and k_p to the linear and the parabolic oxidation constant respectively. The parabolic oxidation constants k_p obtained from this expression for uncoated and coated samples oxidised at 900°C are presented in Table II. For the uncoated substrate oxidised at 950°C, the parabolic constant obtained from a complete law is $k_p = 1.1 \times 10^{-13}$ g^2 cm^{-4} s^{-1}. At 1100°C, the oxidation follows a parabolic law and k_p is 1.3×10^{-13} g^2 cm^{-4} s^{-1} as indicated in Table II. At 1100°C, the mass gain of the coated sample is slightly higher than the one obtained on substrate after 90 hr oxidation at 900°C, but lower than the one observed on the substrate oxidised at 950°C. Moreover, it can be noticed that within the 20 first hours the mass gain of coated sample oxidised at 1100°C is similar to that of coated sample oxidised at 900°C. The scale formed on substrate oxidised at 900°C (Figs. 8a and 9a) is mainly composed of chromia (Cr_2O_3, JCPDS 82-1484). After 48 hr of oxidation, traces of $NiCr_2O_4$ can be observed. For the coated sample oxidised 48 hr at 900°C (Fig. 8b), XRD shows that the diffusion coating composition (Fig. 5) has evolved towards a γ'-Ni_3Al. The oxide scale is only formed by α-Al_2O_3 (JCPDS 10-0173). No trace of θ-Al_2O_3 was found. After 90 hr of oxidation, α-Al_2O_3 is always present but the Ni–Al phases are no more detected. This indicates that all the Al introduced has been consumed by oxidation and diffusion in the metallic matrix. After 90 hr oxidation at

Table II. Parabolic Constant (k_p) of Uncoated and Coated Samples Oxidised in 1 atm. Dry Air Compared with k_p Obtained by Other Authors

$k_p(g^2\,cm^{-4}\,s^{-1})$		This work		An *et al.* [15]	Rybicki *et al.* [32]
samples		uncoated	Coated	β-NiAl coating	NiAl+Zr alloys
Oxidation time		90 hr	90 hr	100 hr	100 hr
Temperature	900°C	7.2×10^{-14}*	8.1×10^{-14}*	9.0×10^{-13}*	6.3×10^{-13}
	1100°C	/	1.3×10^{-13}	1.7×10^{-12}	3.7×10^{-13}

*k_p obtained from a complete law.

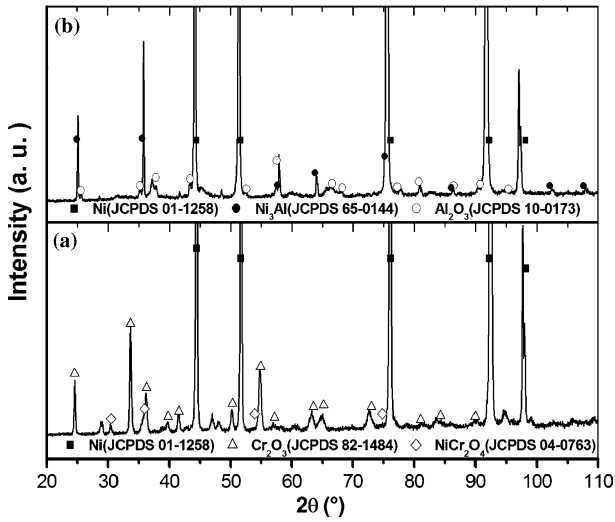

Fig. 8. X-ray diffraction patterns ($K\alpha_{(Cu)}$, θ–2θ) of substrate (a) and coated sample (b) oxidised at 900°C during 48 hr.

1100°C, the oxide scale grown on the coated sample is mainly composed of α-Al_2O_3 (Fig. 9b). At the intermediate 48 hr oxidation time, γ'-Ni_3Al and some traces of mixed (Ni,Al)O oxides were also identified.

Figure 10 shows the typical surface morphologies observed on the Al-coated samples. After 48 hr, respectively at 900 and 1100°C (Fig. 10a, c), the morphology observed after the heat treatment is preserved and some cracks are initiated. After 90 hr at 900°C (Fig. 10b), spallation resulting from the growth and thermal stresses locally occurred. Spalled zones reveal the presence of an intermediate layer, formed of Al-rich whiskers. EDS analysis indicate that the underlayer is composed of oxide grains rich in chromium. No whiskers could be observed on samples oxidised at 1100°C. Nevertheless, the surfaces are rough and strongly spalled (Fig. 10d).

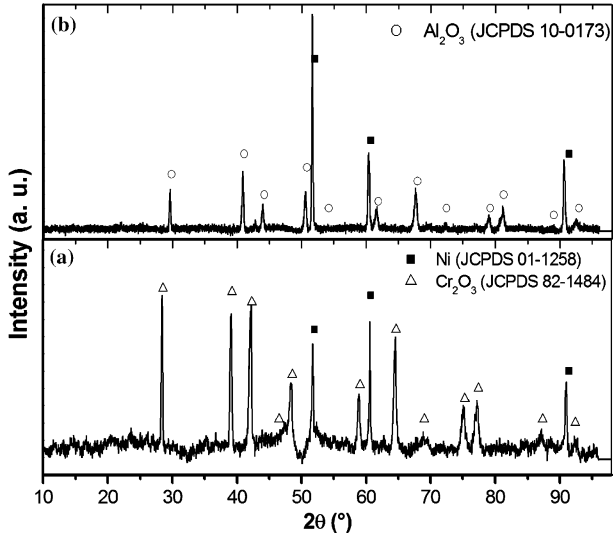

Fig. 9. X-ray diffraction patterns ($K\alpha_{(Co)}$, $\theta = 5°$) of substrate (a) and coated sample (b) oxidised respectively at 900°C and 1100°C during 90 hr.

For the coated sample, after 48 hr oxidation at 900°C and 1100°C, the oxide scale thicknesses are around 3 μm (Figs. 11 and 12), in agreement with the recorded weight gains (Fig. 7). Oxide scales appear constituted of a compact layer at the substrate/oxide interface, surmounted by a less dense layer. After oxidation, the Cr-rich precipitates morphology (Figs. 11 and 12) has changed compared to the one observed after the heat treatment (Figs. 5 and 6), and the chromium precipitate zone is wider. Figures 11b and 12b indicate that the Al diffusion (outer zone) thickness is around 7–8 μm and that Al content is around 18 at.% after 48 hr oxidation at 900°C and at 1100°C. The Al content decreases under the precipitate zone as was also observed after the heat treatment.

For a longer oxidation time (90 hr), EDS analysis (Fig. 13b) reveal only a few percent of Al in the overall analysed zone. The cross section observation (Fig. 13a) of the sample oxidised at 900°C shows the formation of large voids in the internal Al-depleted zone of the diffusion coating and some rod-shaped particles rich in Al. It can also be noticed that the Cr concentration comes back to the original Cr content of the substrate.

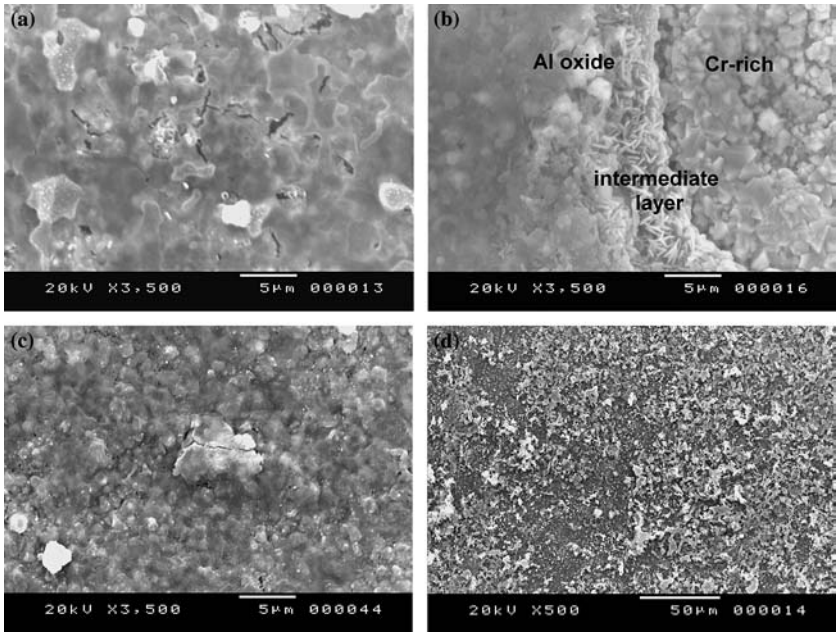

Fig. 10. Surface morphology of coated sample oxidised 48 hr (a), 90 hr (b) at 900°C and 48 hr (c), 90 hr (d) at 1100°C.

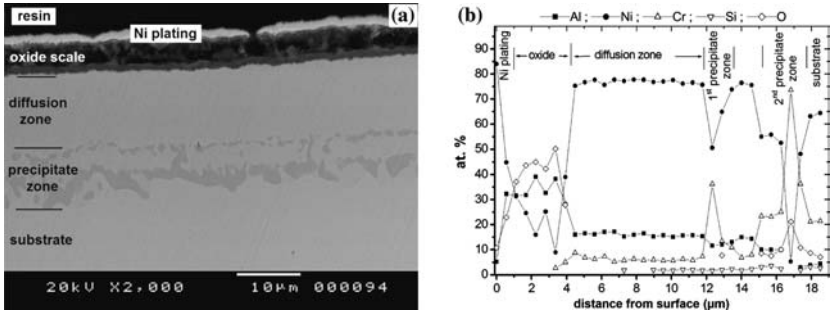

Fig. 11. Cross-section BSE image (a) of Ni-20Cr–1.5Si (wt.%) with 3 μm Al deposit after 48 hr oxidation at 900°C, (b) corresponding EDS concentration profile.

DISCUSSION

Heat Treatment

Formation and growth of intermetallic compounds is governed by diffusion across the growing product phase(s) ("diffusion controlled") and by reaction(s) occurring at the interface ("reaction controlled").[27] In the case of thick films, diffusion finally determines the overall coating growth kinetics.[27,30] The diffusion treatment applied on Al/NiCr alloy diffusion couple (Section Diffusion Treatment) promoted the formation of δ-Ni_2Al_3 ($D5_{13}$ structure[19]) during the first stage at 600°C, while other phases grew in the second stage. The diffusion coating obtained after the second stage at 900°C is a mixture of β-NiAl (B2 structure[18]) with a minor proportion of γ'-Ni_3Al ($L1_2$ structure[25]) and δ-Ni_2Al_3 residual traces while, after treatment at 1100°C, the coating is mainly composed of β-NiAl with an underlying γ'-Ni_3Al layer (biphased

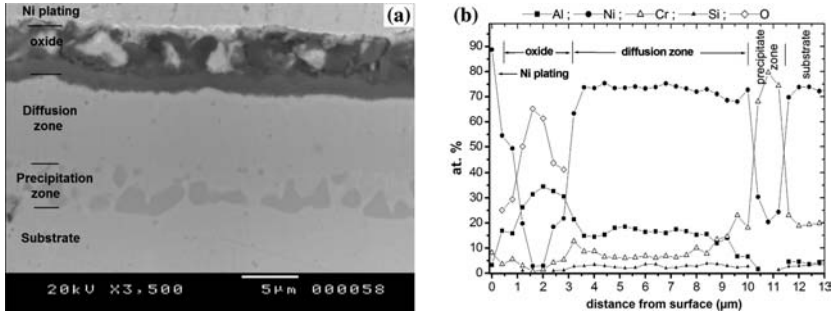

Fig. 12. Cross-section BSE image (a) of Ni-20Cr–1.5Si (wt.%) with 3 μm Al deposit after 48 hr oxidation at 1100°C, (b) corresponding EDS concentration profile.

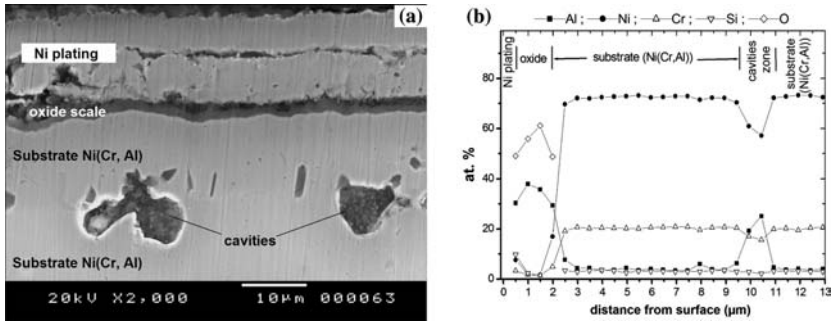

Fig. 13. Cross-section micrograph (SEI) of Ni-20Cr–1.5Si (wt.%) with 3 μm Al deposit after 90 hr oxidation at 900°C.

structure). This diffusion coating composition is close to that of the inward grown coating (two-stage process) obtained by the pack cementation process with high aluminium activity.[9,12,20]

The predominant δ-Ni_2Al_3 brittle phase found after the heat treatment at 600°C (Fig. 3a) is close to the one formed during the first-stage of high aluminium activity coatings, by inward diffusion of Al in a pure Ni, as described by Chien *et al.*[18] These authors found, after a first stage of aluminisation at 850°C, a major δ-Ni_2Al_3layer separated from substrate by Al-rich β-NiAl, Ni-rich β-NiAl, γ'-Ni_3Al and γ-Ni(Al) in an interfacial zone. Janssen *et al.*[30] also observed $NiAl_3$ and δ-Ni_2Al_3 layers formation on Ni–Al sandwich couple annealed at 610°C and show that only aluminium atoms take an important part in the diffusion process during the formation of the $NiAl_3$ and δ-Ni_2Al_3 phase at temperatures around 600°C. More recently, Huang *et al.*[19] studied, by SEM, TEM and EPMA techniques, the microstructure of coating obtained after the first stage of pack cementation aluminizing, of a Ni–Cr alloy, at 750°C. The coating consisted of successive layers which were from substrate to coating: a γ-polygonised zone, an interfacial layer γ /$\gamma' + \alpha$-Cr, $\beta/\delta/\delta+$ Cr_5Al_8. The δ-Ni_2Al_3 phase + Cr_5Al_8 precipitates constituted most of the coating matrix but a high compositional gradient was present near the substrate/coating interface. In the present work, the chromium content analysed by EDS is greater in the substrate than in the coating. This chromium can be involved in a solid solution—such as $Ni_2(Cr,Al)_3$ or $(Ni,Cr)_2Al_3$)—or present as precipitates (α-Cr or Cr_5Al_8[31,32]) too small to be observed by SEM. The other part of Cr is probably expelled out of the δ-Ni_2Al_3matrix.[18] The Al concentration gradient observed in the area close to the diffusion coating/substrate interface may indicate the existence of intermediate Ni–Al phases as the ones previously described.[18]

Further annealing treatments at higher temperatures (900, 1100°C) transformed the brittle δ-Ni_2Al_3 phase principally into γ' and β-NiAl for both temperatures (Fig. 3b,c). Nevertheless, after the second treatment at 900°C, γ'-phase was minor and some residual δ-Ni_2Al_3 traces were detected. After the second stage of aluminising process on pure Ni at 1050°C for 5 h,[18] Chien *et al.* obtained a fine γ' layer at the substrate/coating interface surmounted by a Ni-rich β-NiAl and then a β-NiAl layer. Phase transformation and growth may occur by both inward Al and outward Ni diffusion and finally by dominant Ni diffusion through the coating.[22,30] The Cr-rich zone (Fig. 6a,b) with low Al content was formed during the second-stage of the treatment and Cr content in the diffusion zone decrease in the same time, probably diluted in the thickening coating. The morphology of Cr precipitates changed with temperature suggesting that Cr nuclei have coalesced. The formation of these precipitates can be related to the slow diffusing rate of Cr and the decrease of this element solubility in such Ni–Al system.[12,18,28] Tian *et al.*[32] found a maximum solid solubility of Cr in β-NiAl around 8 at.% at 1563 K with a decrease of this

value with decreasing the temperature. At room temperature the solubility of chromium is around 4 at.%.[31]

The phases formed after each stage of the applied heat treatment under Ar gas atmosphere can be summarised in the following sequences:

$$\mathrm{Al} + \gamma\text{-Ni(Cr)} \xrightarrow{600^\circ\mathrm{C}/1\,\mathrm{h}} \delta\text{-Ni}_2(\mathrm{Al, Cr})_3 + \gamma\text{-Ni(Cr)} \quad \text{followed by}$$
$$\xrightarrow{900^\circ\mathrm{C}/15\,\mathrm{min}} \beta\text{-Ni(Al, Cr)} + \varepsilon(\gamma'\text{-Ni}_3(\mathrm{Al, Cr}) + \delta\text{-Ni}_2(\mathrm{Al, Cr})_3)$$
$$+\mathrm{Cr_{rich}\,precipitate} + \gamma\text{-Ni(Cr)}$$

or by

$$\xrightarrow{1100/15\,\mathrm{min}} \beta\text{-Ni(Al, Cr)} + \gamma'\text{-Ni}_3(\mathrm{Al, Cr}) + \mathrm{Cr_{rich}\,precipitates} + \gamma\text{-Ni(Cr, Al)}$$

where γ-Ni(Cr) corresponds to the solid solution of Ni–20wt.%Cr and ε symbol to the traces of intermetallics phases detected during experiments. The $\mathrm{Ni}_x(\mathrm{Al,Cr})_y$ notation has been chosen to indicate the presence of Cr in solid solution, as mentioned before.

Alumina was not included in this sequence despite the unwanted oxidation which occurred during this heat treatment.

High Temperature Oxidation

Ni-20%Cr is well known to form three possible oxide phases (NiO, $NiCr_2O_4$ and Cr_2O_3)[2–4] but XRD analysis of oxidised uncoated sample (Figs. 8a and 9a) did not permit to identify nickel oxide and only small traces of $NiCr_2O_4$ were detected. This can probably be attributed to the silicon content (1.5wt.%) in the alloy, in agreement with Ahmad and Fox[1] who demonstrated the formation of a thin amorphous silica layer at the scale/alloy interface, below a chromia scale. This silica layer strongly decreases the O_2 partial pressure at the metal oxide interface, so that nickel cannot be oxidised during the initial oxidation stage. In the present study, the mass gain observed at 900°C is three times smaller in comparison with Calvarin *et al.* results,[2] obtained after 96 hr of oxidation of Ni–20%Cr alloy without silicon. This is probably related to the absence of NiO formation during the initial stage of oxidation.

Heat treatment applied on coated samples produces rich-aluminide diffusion coatings, at 900°C, with an overall coating composition around 40 wt.% and two-phase β-NiAl + γ'-Ni_3Al microstructure, at 1100°C, with an Al content comprised between 33 at.% and 13 at.% and a Cr content around 10%. The γ'-Ni_3Al is likely to form NiO, and $NiAl_2O_4$, or a metastable γ-Al_2O_3 layer above an α-Al_2O_3 healing layer during the

fast-growth transient stage of oxidation depending on the γ'-phase type (alloys[33–35] or diffusion coating[16]) and on the oxidation temperature. The case of β-NiAl (alloys or diffusion) coating is different due to their higher Al contents. The transient stage of oxidation on β-NiAl results in the formation of metastable phases, such as θ-Al_2O_3, which growth rates are comparable to those encountered in the case of the transient scales on γ'-Ni_3Al as the growth is controlled by outward diffusion of Al ions.[14,34] The metastable Al_2O_3 phases are transformed, after an incubation time, into thermodynamically stable α-Al_2O_3. Different authors indicate that this transformation, thermally activated,[14,36] is accompanied by changes in oxidation kinetics[7,35] and scale morphologies.[7,8] Ribicky and Smialek[36] showed in their study on isothermal oxidation of β-NiAl+Zr that at low temperatures ($<1000°C$) and high temperatures ($>1000°C$) weight gain curves follow parabolic kinetics corresponding to the growth of θ-Al_2O_3 and α-Al_2O_3, respectively. At intermediate temperature (around 1000°C), they observed change in growth rate after a few hours of oxidation, corresponding to the transition from fast-growth (θ-Al_2O_3) to slow-growth alumina phase (α-Al_2O_3).

In the present study, the kinetic curves have been analysed with a complete law at 900°C and with a parabolic one at 1100°C. For both oxidation temperatures, only α-Al_2O_3 (JCPDS 10-0173) was detected by XRD (Figs. 8b and 9b) after 48 hr and 90 hr of oxidation. No trace of θ-Al_2O_3 phase was detected by XRD. However the whiskered morphology of the intermediate oxide scale observed on sample oxidised at 900°C (Fig. 10b) is in agreement with the morphology described for θ-Al_2O_3 growth[7] resulting from the fast outward-Al diffusion mechanism. The significant weight gain recorded during the initial oxidation time on coated samples oxidised at 900°C may also indicate the formation of a fast-growing θ-Al_2O_3 at this temperature. In the case of α-Al_2O_3, it is generally admitted that both oxygen and cation diffusion contribute to the growth with an important role played by inward oxygen diffusion through scale grain boundaries.[7,37,38] According to Ribicky and Smialek[36] observations, the whiskers topography changed into flat plates with radial cracks and, eventually, into a network of ridges, growing through different diffusion mechanisms occurring simultaneously. The transition of the metastable alumina layer formed on β-NiAl during the initial stage of oxidation influences the final ridge-type morphology of the α-Al_2O_3, as it is proposed by Hindam *et al.*[36] Pint *et al.*[39] consider that this morphology is due to the formation of fine grains (intrinsic structure) by outward diffusion of Al along Al_2O_3 scale grain boundaries and of large grains (extrinsic) ridge morphology resulting from the cracking during the phase transformation. Consequently, the scale morphology is different

and the ridge-type network does not exist when the phase transformation is inhibited. The presence of chromium in the alumina-forming phases influences the initial stage of oxidation, particularly by promoting the θ-$Al_2O_3 \rightarrow \alpha$-$Al_2O_3$ transformation.[13,34,35] Cr_2O_3 nuclei could form a mixed oxide $(Cr,Al)_2O_3$, with the metastable alumina, which can act as nucleation site for the hexagonal α-Al_2O_3.[38,31] Brumm and Grabke[40] indicate that transformation of θ-Al_2O_3 into α-Al_2O_3 is very slow at 900°C: traces of α-Al_2O_3 were observed on β-NiAl after 60 hr of oxidation while the transformation occurred after only 10 hr on NiAl–Cr alloys. Therefore, the observation of chromium rich grains (Fig. 10b) and small increase of Cr content analysed at the oxide scale/interface (Figs. 11b and 12b) would corroborate this assumption. Table II shows that the oxidation parabolic constants obtained on sample oxidised at 900°C and 1100°C are consistent with the ones encountered in the literature.[15,37,40]

After 100 hr of oxidation, the upper part of the scale is partially spalled and no voids are observed at the remaining scale/metal interface (Fig. 13). Numerous mechanisms have been proposed to describe voids formation at the oxide scale interface[7,32] but Liu *et al.*[35,41] mention that fast $\theta \rightarrow \alpha$-$Al_2O_3$ transformation prevents the formation of interfacial voids, well known to play a major role in the scale spallation. In addition, large cavities are observed at the Al depleted zone/NiCr substrate interface resulting from the evolution of the diffusion coating composition during oxidation process. The Al contained into the diffusion coating was consumed by oxide scale formation and by further diffusion and dilution into the alloy.[42] Then, Cr solubility in the Al-depleted zone tended to increase and cavities were formed as a result of the Cr-rich precipitate dissolution.

Evolution of the diffusion coating phases and oxide scale formed during the oxidation process at both temperatures can then be summarised in the following sequences:

$$\xrightarrow{0.2\,\text{atm}\,O_2/48\,\text{h}} \alpha\text{-}Al_2O_3 + \gamma'\text{-}Ni_3(Al, Cr) + Cr_{\text{rich}}\,\text{precipitate} + \gamma\text{-}Ni(Cr, Al)$$

$$\xrightarrow{0.2\,\text{atm}\,O_2/90\,\text{h}} \alpha\text{-}Al_2O_3 + \text{large cavities} + \gamma\text{-Ni(Cr,Al)}$$

where γ-Ni(Cr,Al) corresponds to the NiCr solid solution with small addition of Al.

CONCLUSION

In this study, NiCr alloy samples have been coated with 3 μm Al films by magnetron sputtering. Diffusion aluminide coatings were then formed through a two-stage heat treatment under inert gas atmosphere, the first

one at 600°C and the second at 900 or 1100°C. Aluminides obtained at 900°C and 1100°C are close to those obtained by pack cementation process with high aluminium activity. At both temperatures, the phase formed after the whole heat treatment was mainly composed of β-NiAl and γ'-Ni_3Al, containing Cr. More, a Cr-rich precipitates zone was observed at the diffusion coating/substrate interface. After 48 hr of oxidation at both temperatures, only $\alpha' Al_2O_3$ and γ'-Ni_3Al could be detected. An intermediate scale, with a whiskered morphology, was observed after oxidation at 900°C. After 90 hr of oxidation, the upper part of the oxide scale spalled during cooling and the Ni_xAl_y phases formed during heat treatment totally disappeared. Large cavities, attributed to dissolution of Cr in the Al depleted matrix, were observed at the initial location of the Cr-rich precipitates. The beneficial effect of the aluminide diffusion coating on high-temperature behaviour of NiCr was pointed out in the case of coated sample oxidation at 1100°C. The weight gain recorded at this temperature is actually smaller than the one for the uncoated NiCr at 950°C.

REFERENCES

1. B. Ahmad and P. Fox, *Oxidation of Metals* **52**, 113 (1999).
2. G. Calvarin, A. M. Huntz, and R. Molins, *Material High Temperature* **17**(2), 257 (2000).
3. A. Ul-Hamid, *Material Chemistry and Physics* **80**, 135 (2003).
4. D. P. Whittle and J. Stringer, *Philosophical Transactions of the Royal Society of London Series A* **295**, 309 (1980).
5. T. Amano, S. Yajima, and Y. Saito, *Transactions of the Japan Institute of Metals* **26**, 433 (1985).
6. A. Ul-Hamid, *Oxidation of Metals* **46**, 27 (2004).
7. F. H. Stott, *Materials Science Forum* **251–254**, 19 (1997).
8. F. A. Golightly, F. H. Stott, and J. C. Wood, *Journal Electrochemical Society* **126**, 1035 (1979).
9. G. W. Goward, *Surface Coatings Technology* **108–109**, 73 (1998).
10. E. Basuki, A. Crosky, and G. Gleeson, *Materials Science and Engineering* **A224**, 27 (1997).
11. F. J. Pérez, F. Pedraza, M. P. Hierro, J. Balmain, and G. Bonnet, *Surface Coatings Technology* **153**, 49 (2002).
12. J. Angenete and K. Stiller, *Surface Coatings Technology* **150**, 107 (2002).
13. J. A. Smialek, *Metallurgical Transactions* **A9**, 309 (1978).
14. R. Bianco, R. A. Rapp, and J. Smialek, *Journal of the Electrochemical Society* **140**, 1191 (1993).
15. T. F. An, H. R. Guan, X. F. Sun, and Z. Q. Hu, *Oxidation of Metals* **54**, 301(2000).
16. D. F. Susan and A. R. Marder, *Oxidation of Metals* **57**, 159 (2002).
17. L. Levin, A. Ginzburg, L. Klinger, T. Werber, A. Katsman, and P. Schaaf, *Surface Coatings Technology* **106**, 209 (1998).
18. A. Chien, G. Gan, and P. Shen, *Materials Science and Engineering* **A272**, 207 (1999).
19. H. L. Huang, Y. Z. Chen, and D. Gan, *Materials Science and Engineering* **A328**, 238 (2002).
20. A. Chien, G. Gan, and P. Shen, *Materials Science and Engineering* **A206**, 215 (1996).
21. F. J. Pérez, M. P. Hierro, F. Pedraza, C. Gomez, M. C. Carpintero, and J. A. Trilleros, *Surface Coatings Technology* **122**, 281 (1999).

22. N. Voudouris, Ch. Christoglou, and G. N. Angelopoulos, *Surface Coatings Technology* **141**, 275 (2001).
23. B. Ning and M. L. Weaver, *Surface Coatings Technology* **177-178**, 113 (2004).
24. S. Yang, F. Wang, Z. Sun, and S. Zhu, *Intermetallics* **10**, 467 (2002).
25. J. L. He, C. H. Yu, A. Leyand, A. D. Wilson, and A. Matthews, *Surface Coatings Technology*. **155**, 67 (2002).
26. M. S. Chu and S. K. Wu, *Acta Materiala* **51**, 3109 (2003).
27. H. Mehrer, *Materials Transactions, JIM* **37**, 1259 (1996).
28. R. Mevrel and R. Pichoir, *Materials Science and Engineering* **88**, 1 (1987).
29. M. F. Singleton, J. L. Murray, and P. Nash, in: *Binary alloy phase diagrams*, T. B. Massalski, ed. (American Society for Metals, Metals Park (OH) 1986) p. 140.
30. M. M. P. Janssen and G. D. Rieck, *Transactions Metallurgical Society of AIME* **239**, 1372 (1967).
31. S. Merchant and M. R. Notis, *Materials Science and Engineering* **66**, 47 (1984).
32. W. H. Tian, C. S. Han, and M. Nemoto, *Intermetallics* **7**, 56 (1999)
33. Z. Liu and W. Gao, *Intermetallics* **8**, 1385 (2000).
34. J. A. Horton, J. V. Cathcart, and C. T. Liu, *Oxidation of Metals* **29**, 347 (1988).
35. Z. Liu and W. Gao, *Oxidation of Metals* **55**, 481 (2001).
36. G. C. Rybicki and J. L. Smialek, *Oxidation of Metals* **31**, 275 (1989).
37. H. M. Himdam and W. W. Smeltzer, *Journal of Electrochemical Society* **127**, 1630 (1980).
38. J. Balmain, M. K. Loudjani, and A. M. Huntz, *Materials Science and Engineering* **A224**, 87 (1997).
39. B. A. Pint, M. Treska, and L. W. Hobbs, *Oxidation of Metals* **47**, 1 (1997).
40. M. W. Brumm and H. J. Grabke, *Corrosion Science* **33**, 1677 (1992).
41. Z. Liu and W. Gao, *Oxidation of Metals* **54**, 189 (2000).
42. E. Basuki, A. Crosky, and B. Gleeson, *Materials Science and Engineering* **A224**, 27 (1997).